Acinar cell clonal expansion in pancreas homeostasis and carcinogenesis

Patrick Neuhöfer[1,2,3], **Caitlin M. Roake**[1,2,3], **Stewart J. Kim**[1,2,3], **Ryan J. Lu**[1,2,3], **Robert B. West**[4], **Gregory W. Charville**[4], **Steven E. Artandi**[1,2,3]

[1]Stanford Cancer Institute, Stanford University School of Medicine, Stanford, CA, USA.

[2]Department of Medicine, Stanford University School of Medicine, Stanford, CA, USA.

[3]Department of Biochemistry, Stanford University School of Medicine, Stanford, CA, USA.

[4]Department of Pathology, Stanford University School of Medicine, Stanford, CA, USA.

Abstract

Pancreatic ductal adenocarcinoma (PDAC) is one of the leading causes of cancer deaths worldwide[1]. Studies in human tissues and in mouse models have suggested that for many cancers, stem cells sustain early mutations driving tumour development[2,3]. For the pancreas, however, mechanisms underlying cellular renewal and initiation of PDAC remain unresolved. Here, using lineage tracing from the endogenous telomerase reverse transcriptase (*Tert*) locus, we identify a rare TERT-positive subpopulation of pancreatic acinar cells dispersed throughout the exocrine compartment. During homeostasis, these TERT^high acinar cells renew the pancreas by forming expanding clones of acinar cells, whereas randomly marked acinar cells do not form these clones. Specific expression of mutant *Kras* in TERT^high acinar cells accelerates acinar clone formation and causes transdifferentiation to ductal pre-invasive pancreatic intraepithelial neoplasms by upregulating Ras–MAPK signalling and activating the downstream kinase ERK (phospho-ERK). In resected human pancreatic neoplasms, we find that foci of phospho-ERK-positive acinar cells are common and frequently contain activating *KRAS* mutations, suggesting that these acinar regions represent an early cancer precursor lesion. These data support a model in which rare TERT^high acinar cells may sustain *KRAS* mutations, driving acinar cell expansion and creating a field of aberrant cells initiating pancreatic tumorigenesis.

PDAC is derived from epithelial cells within the exocrine pancreas, which comprise secretory acinar cells and duct cells[4]. Exocrine pancreas cells are lineage-restricted in that

newly generated acinar cells and ductal cells derive primarily from the acinar cell and ductal cell compartments, respectively[5]. Within the acinar cell lineage, rare subsets of acinar cells are thought to fuel acinar renewal[6,7]. PDAC cancer cells exhibit a ductal fate and PDAC is frequently derived from pre-invasive pancreatic intraepithelial neoplasm (PanIN) lesions with ductal identity[8]. Despite these ductal features, genetic studies using mouse models support an origin for PDAC and PanINs in the acinar compartment[9–12]. By contrast, studies using mouse and human organoids indicate that genetic manipulation of ductal organoids yields PanIN lesions and PDAC after orthotopic transplantation[13,14]. Mutational activation of *KRAS* is the dominant pathway driving development of PDAC and PanIN, and *KRAS* mutations are found in 95% of invasive PDAC and 68–90% of PanINs[15,16]. *KRAS* mutation is sufficient to drive PanIN formation, whereas loss of tumour suppressor genes is required for progression to PDAC[17–19]. Telomerase serves essential functions in stem cell self-renewal and in carcinogenesis through its role in adding DNA repeats to telomeres, nucleoprotein structures that protect chromosome ends. Insufficient levels of telomerase lead to progressive telomere shortening, culminating in senescence and crisis responses[20]. In many tissues, telomerase expression is restricted to stem cell and progenitor cell populations, based on transcriptional control of *Tert*[21]. In pancreas, telomerase is universally upregulated in invasive PDAC, and polymorphisms in the *TERT* locus are linked to increased PDAC risk[22], but *Tert* expression patterns in normal pancreas have not been explored.

Results

Rare acinar cells with elevated *Tert* mRNA

To identify *Tert*-expressing cells and to understand mechanisms of cellular renewal in the pancreas in vivo, we used lineage tracing with a mouse strain expressing the regulated CreERT2 recombinase from the endogenous *Tert* locus[23] (Extended Data Fig. 1a). We intercrossed *Tert*$^{CreERT2/+}$ mice and a *Rosa26*$^{LSL-Tomato/+}$ reporter strain that results in Cre-dependent permanent cell labelling by expression of fluorescent Tomato protein (Extended Data Fig. 1b). Adult *Tert*$^{CreERT2/+}$; *Rosa26*$^{LSL-Tomato/+}$ (*Tert-CreER*) mice were injected with a single dose of tamoxifen (5 mg) and analysed after 10 days to label cells that actively express *Tert* (Fig. 1a, b, Extended Data Fig. 1a). We found that a rare subset of cells dispersed throughout the pancreas expressed Tomato. Double immunostaining revealed that within the exocrine pancreas, Tomato-positive cells were exclusively amylase-positive acinar cells, whereas ductal cells expressing Tomato were not detected (Fig. 1c, Extended Data Fig. 1c, g). In the islets, a subset of rare Tomato-positive β-cells was identified (Extended Data Fig. 1d).

To determine whether *Tert* mRNA is enriched in rare Tomato-positive cells, Tomato$^+$ and Tomato$^-$ acinar cells from *Tert-CreER* mice and bulk acinar cells from wild-type mice sorted by fluorescence-activated cell sorting (FACS) were analysed for *Tert* mRNA expression using single-molecule RNA fluorescence in situ hybridization (FISH) (Fig. 1d, e, Extended Data Fig. 1e, f, Supplementary Information). Quantification of mRNA FISH demonstrated that the vast majority of bulk acinar cells were TERT^{low}, while a rare subpopulation (1.9%) was TERT^{high}. Tomato$^-$ cells from *Tert-CreER* mice closely resembled bulk cells from wild-type mice. By contrast, Tomato$^+$ cells were highly enriched for TERT^{high} cells (Fig.

1f). Additionally, Tomato^{+} cells expressed higher levels of acinar markers and *Tert* mRNA —as detected by quantitative PCR with reverse transcription (RT–qPCR)—compared with Tomato^{−} cells (Extended Data Fig. 1h). In comparing the identity of the TERT^{high} cells with previously published subsets of acinar cells, we found that TERT^{high} cells expressed neither BMI1 nor DCLK1 by immunofluorescence[6,7] (Extended Data Fig. 1i, j). These data identify a rare acinar cell subpopulation with elevated levels of *Tert* mRNA distributed throughout the exocrine pancreas.

TERT^{high} acinar cells renew the pancreas

To determine whether TERT^{high} acinar cells repopulate the pancreas during homeostasis, we performed long-term tracing experiments in adult *Tert-CreER* mice analysed 6–24 months after tamoxifen injection (Extended Data Fig. 2a). During this time course, the average clone size increased progressively as single-cell clones diminished in abundance, whereas multi-cell clones increased (Fig. 2a, c, d). These data show that TERT^{high} acinar cells repopulate the exocrine pancreas and yield progressively expanding clones for up to two years.

To understand whether this clone-forming ability is restricted to TERT^{high} acinar cells, we randomly labelled acinar cells in the pancreas using the mouse strain *Ptf1a^{CreERT2/+}*, which expresses CreER specifically in acinar cells, and titrated tamoxifen doses (0.05–5 mg) to assess labelling efficiency (Extended Data Fig. 2b–d). Treatment of adult *Ptf1a^{CreERT2/+}; Rosa26^{LSL-Tomato/+}* (*Ptf1a-CreER*) mice with 0.05 mg tamoxifen yielded sparse, single-cell labelling that approximated the frequency of acinar cells marked in *Tert-CreER* mice. To compare the clone-forming abilities of TERT^{high} acinar cells and random acinar cells, we treated *Ptf1a-CreER* mice with 0.05 mg tamoxifen, followed by tracing for 10 days, 6 months and 12 months (Fig. 2b). In contrast to the clonogenicity of TERT^{high} acinar cells, randomly labelled acinar cells did not form clones even after a 12-month trace (Fig. 2d, Extended Data Fig. 2e).

We assessed rates of proliferation of TERT^{high} acinar cells and TERT^{low} acinar cells by exposing tamoxifen-treated *Tert-CreER* mice to bromo-deoxyuridine (BrdU) in the drinking water for four weeks (Extended Data Fig. 2f). Consistent with the clone-forming ability of TERT^{high} acinar cells, BrdU incorporation was approximately fourfold higher in TERT^{high} acinar cells compared with unlabelled TERT^{low} acinar cells (Extended Data Fig. 2g, h). *Tert* mRNA FISH on FACS-purified Tomato^{+} acinar cells isolated from *Tert-CreER* mice showed that the representation of high *Tert* mRNA cells decreased from 79.7% to 39.0% comparing the 10-day and one-year tracing, indicating that clone formation by TERT^{high} acinar cells is characterized by an increasing number of TERT^{low} acinar cells, while a subpopulation of TERT^{high} acinar cells is retained to fuel further clonal expansion (Fig. 2e, Extended Data Fig. 2i–k).

The acinar compartment has capacity for accelerated regeneration in the setting of chemical injury[5]. To understand how TERT^{high} acinar cells contribute to injury responses, we induced pancreatitis using cerulein in cohorts of *Tert-CreER* mice and *Ptf1a-CreER* mice (Extended Data Fig. 3a). TERT^{high} cells showed accelerated clone formation at both 10 days and 30 days compared with randomly marked acinar cells in *Ptf1a-CreER* mice (Fig. 2f, g).

Consistent with the enhanced clone formation of TERT^{high} cells in the context of cerulein-induced injury, the frequency of Ki-67 expression was greater in Tomato-positive cells than in the bulk population of Tomato-negative acinar cells at days 10 and 30 (Extended Data Fig. 3b, c). Inducing pancreatic injury with L-arginine treatment caused an increase in the size of TERT[high] acinar cell-derived Tomato[+] clones compared with untreated controls (Extended Data Fig. 3d–f). Taken together, these data indicate that TERT^{high} acinar cells renew the acinar cell compartment by forming clones that are increasingly comprised of TERT^{low} acinar cells and that this capacity for self-renewal is more limited in the general acinar cell population.

PanINs driven by KRAS in TERT^{high} cells

Activating mutations in *KRAS* are commonly associated with human PanINs and are sufficient to induce PanIN formation in mice[18]. In mouse genetic studies, *Kras* is typically activated throughout the acinar compartment, or throughout the pancreas, resulting in widespread transformation of the normal pancreas to PanINs within a week after cerulein treatment[24]. To model clonal activation of KRAS in a way that may more closely approximate events in humans, we assessed the effects of activating Kras specifically in rare TERT^{high} acinar cells. To this end, we intercrossed *Tert-CreER* mice together with a conditional Cre-dependent mutant *Kras* G12D strain, generating *Tert[CreERT2/+]; Kras[LSL-G12D/+]; Rosa26[LSL-Tomato/+]* (*Tert-CreER; Kras*) mice. For comparison, we measured the effect of activating KRAS in random acinar cells by intercrossing the same conditional Kras strain with *Ptf1a-CreER* mice to yield *Ptf1a[CreERT2/+]; Kras[LSL-G12D/+]; Rosa26[LSL-Tomato/+]* (*Ptf1a-CreER; Kras*) mice. Both cohorts of mice were treated with tamoxifen, followed by repeated injections of cerulein to induce pancreatitis (Extended Data Fig. 4a). Analysis at 30 days after cerulein treatment revealed an increase in acinar cell clone size in *Tert-CreER; Kras* mice compared with *Ptf1a-CreER; Kras* mice. Acinar cell clone size for *Ptf1a-CreER; Kras* mice at 3 months remained significantly lower than for *Tert-CreER; Kras* mice at 1 month. In addition, mutant Kras caused enhanced clone formation when expressed in TERT^{high} cells, comparing labelled clones in *Tert-CreER; Kras* mice with those in *Tert-CreER* mice. These effects of mutant *Kras* in accelerating acinar clone formation were seen both in mice treated with cerulein and in those that remained untreated (Fig. 3b).

To compare the effects of Kras in promoting transdifferentiation and transformation in TERT^{high} cells compared with random acinar cells, we assessed the frequency of ductal metaplasia and PanIN formation in both cohorts. Metaplastic area (Extended Data Fig. 4d) and PanIN area (Extended Data Fig. 4e) were both significantly increased in *Tert-CreER; Kras* mice after one month compared with *Ptf1a-CreER; Kras* mice after one month and 3 months (Fig. 3a, c, d, Extended Data Fig. 4h–k). The number of acinar clones per unit area was not significantly different between the two experimental cohorts, indicating that the increased incidence of metaplastic area and PanINs in *Tert-CreER; Kras* mice was not owing to a higher number of clones expressing mutant Kras (Extended Data Fig. 4b, c). Of note, treatment with a high dose of tamoxifen (5 mg) in *Ptf1a-CreER; Kras* mice led to complete transformation of the pancreas one month after injury, as previously described[24]

(Extended Data Fig. 4f, g). PanINs were evident by ductal morphology, prominent apical mucin, staining for Alcian blue and MUC5A (Fig. 3a, c, d, Extended Data Fig. 4e).

Mutational activation of KRAS causes persistent activation of downstream signalling pathways including MAPK and PI3K[25]. Consistent with engagement of MAPK, invasive PDAC and PanIN typically express the activated, phosphorylated forms of the downstream protein kinases MEK and ERK. MAPK signalling is important for PanIN formation in Kras-driven mouse models of pancreas cancer[26]. To investigate MAPK signalling in the progression from acinar clone to PanIN, we stained sections using antibodies against phospho-ERK1/2, the ductal marker CK19, and Tomato. pERK was undetectable in small acinar clones with fewer than ten cells per clone (Fig. 3f), whereas it was readily detected in larger acinar clones derived from TERT^{high} acinar cells (Fig. 3g). In PanIN lesions, the pERK signal was further elevated, whereas Tomato levels diminished, perhaps reflecting downregulation of the ubiquitous promoter directing Tomato expression in the ductal state (Fig. 3h).

Additionally, daily oral administration of the MEK inhibitor trametinib in *Tert-CreER; Kras* mice after pancreatitis inhibited the formation of PanINs and TERT[high] acinar clone size was reduced (Extended Data Fig. 5). This supports the notion that MAPK signalling is needed for the formation and maintenance of PanIN lesions[26]. Our data indicate that mutant *Kras* activation in TERT^{high} acinar cells coupled with injury leads to acinar clonal expansion, progressive pERK upregulation and subsequent formation of PanIN lesions (Fig. 3i).

KRAS mutations in human pERK^{+} acinar cells

To investigate whether acinar cell expansion is a potential early step in pancreatic tumorigenesis, we assayed pERK staining in resected pancreas specimens from patients with PDAC, patients with chronic pancreatitis and patients with either serous cystadenoma (SCA) or mucinous cystic neoplasm (MCN) (Extended Data Table 1). Resected human PDAC samples were evaluated by a pathologist to identify tissue blocks containing PanINs together with adjacent acinar tissue. We found that PanINs were commonly positive for pERK, whereas most acinar tissue and islets were pERK[−] (Fig. 4a, Extended Data Fig. 6). In staining sections from 38 patients, we identified pERK[+] acinar foci in a total of 20 patients (Fig. 4b). Pancreas autopsy samples from individuals without pancreatic disease showed no pERK[+] acinar foci (Fig. 4b). These findings indicate the common presence of pERK[+] acinar foci in resected pancreas specimens from patients with PDAC, other neoplastic processes and chronic pancreatitis.

KRAS mutations in acinar cells or in duct cells have not been detected, making the origin of PanINs in humans unclear. To understand whether these pERK[+] acinar foci contained *KRAS* mutations, we performed laser capture microdissection (LCM), followed by PCR amplification of the 5′ portion of the *KRAS* gene and next generation sequencing. LCM was performed on stained sections to specifically isolate pERK[+] acinar foci and pERK[−] acinar regions from the same patient whenever possible (Extended Data Table 2). *KRAS* mutations were detected in 5 out of 18 pERK[+] acinar regions isolated from resected, diseased pancreata. The mutations identified were exclusively G12D, the most common *KRAS* mutation in human pancreas cancer[27] (Fig. 4c, d). Allelic frequencies of the

mutations ranged from 19.9% to 73.1%. As controls, we randomly sampled pERK⁻ acinar cell regions from the diseased pancreata and the autopsy cases. We found that 32 out of 34 samples showed only wild-type *KRAS* sequences, however, two mutant *KRAS* sequences were identified in the pERK⁻ samples. Together, these data reveal the presence of pERK⁺ acinar foci in samples of patients with pancreatic diseases. Additionally, these pERK⁺ acinar foci are enriched for the presence of activating mutations in *KRAS* suggesting pERK as a potential marker for *KRAS* mutations within the acinar cell compartment (Fig. 4e).

Discussion

Our findings provide support for a unified model linking renewal mechanisms in the exocrine pancreas to initiation of pancreatic carcinogenesis. During homeostasis, rare TERT^high acinar cells fuel acinar cell renewal by producing expanding clones, but during chemical injury this process is accelerated while additional acinar cells are also recruited to form clones. Our data suggest that if TERT^high acinar cells sustain a *Kras* mutation during replication, this mutation in turn confers a selective growth advantage yielding expanding clones of premalignant cells that initially retain acinar morphology. The expansion of these premalignant acinar cell clones would represent an abnormal field serving as a reservoir for the accumulation of additional genetic and epigenetic changes necessary for transdifferentiation to the PanIN fate and ultimately for generation of a fully transformed cancer. Our findings of pERK⁺ acinar foci that contain *KRAS* mutations in human PDAC samples support this acinar clonal expansion hypothesis. The identification of *KRAS* mutations in acinar foci is consistent with emerging data indicating the presence of cancer gene mutations in normal-appearing cells in aging tissues[28–30]. Chronic organ damage such as in pancreatitis increases the proliferation of acinar progenitor cells and the likelihood of developing a KRAS mutation, while further enhancing the growth of KRAS-mutant clones and the risk of PDAC development. The identification of this acinar cell expansion step in PDAC development suggests methods for early interception of pancreatic cancer.

Online content

Any methods, additional references, Nature Research reporting summaries, source data, extended data, supplementary information, acknowledgements, peer review information; details of author contributions and competing interests; and statements of data and code availability are available at https://doi.org/10.1038/s41586-021-03916-2.

Methods

Mice

Tert^CreERT2/+ mice were intercrossed with the *Rosa26* reporter (Gt(ROSA) 26Sortm14(CAG-tdTomato)Hze/J) line to generate *Tert^CreERT2/+; Rosa26^LSLTomato/+* mice for analysis[23,31]. Additionally, those mice were bred with *Kras^LSL-G12D/+* mice generating *Tert^CreERT2/+; Kras^LSL-G12D/+; Rosa26^LSLTomato/+* mice[32]. Two-month-old mice were gavaged with tamoxifen (Cayman, between 0.05 mg to 3 × 5 mg per mouse) dissolved in 100 μl sesame oil (Sigma-Aldrich). Sparse labelling in *Ptf1a^CreERT2/+; Rosa26^LSLTomato/+* mice was achieved by injecting 0.05 mg of tamoxifen intraperitoneally into 2-month-

old mice[33]. *Ptf1a^{CreERT2/+}; Kras^{LSL-G12D/+}; Rosa26^{LSLTomato/+}* mice were bred with *Kras^{LSL-G12D/+}* mice, generating *Ptf1a^{CreERT2/+}; Rosa26^{LSLTomato/+}* mice. BrdU (Sigma) was administrated via drinking water (1 mg ml^{-1}) for the indicated time frame.

For acute pancreatitis injury, 2-month-old mice were fasted for 12–18 h and injected with cerulein (Sigma, 100 mg kg^{-1} body weight) every hour for 8 h on 2 consecutive days. Trametinib (1 mg kg^{-1} body weight, Selleckchem) or vehicle was administered orally every day for 30 days with the first dose one hour after the last injection of cerulein on day 1 of pancreatitis. L-Arginine pancreatitis was induced by three injections of 10% L-arginine (3 mg; Sigma)[34]. Male and female mice were randomly divided into the different experimental groups with at least three mice per group. Sample size was estimated based on expected magnitude of change using statistical methods. All experiments were repeated at least twice. Mice were housed in 22 °C ambient temperature and 40% humidity, with a 12-hour light:dark cycle (07:00–19:00). Tumour size of 1.5 cm in diameter or other endpoints approved were not exceeded. All animal protocols were approved by the Institutional Animal Care and Use Committee at Stanford University (APLAC-12684).

Immunohistochemistry and immunofluorescence

Pancreata were fixed in 10% buffered-formalin (Fisher scientific). For immunofluorescence, tissue was fixed overnight, cryoprotected in 30% (w/v) sucrose, embedded in OCT, snap-frozen and cut into 8-μm cryosections.

For immunohistochemistry, tissue was fixed overnight at room temperature, incubated in 70% ethanol overnight, embedded in paraffin and cut into 5-μm sections. Antigen retrieval was performed with citrate buffer (pH 6; Vector Laboratories) for 10 min using a pressure cooker. Slides were stained with primary and secondary antibodies in blocking buffer (5% goat serum, 0.3% Triton-X100 in PBS or TBS) overnight at 4 °C, incubated with 1 mM DAPI for 5 min at room temperature, and mounted in Aqua poly/mount (Polysciences) or Vectashield with DAPI (Vector laboratories). DAB Peroxidase Substrate Kit (Vector Laboratories) was used for immunohistochemistry.

The following antibodies were used in this study: anti-CK19 (Hybridoma Bank, TROMA-III, 1:100–1:500); anti-RFP (Abcam, ab124754, 1:500–1:1,000); anti-RFP (MBL, M208–3, 1:200); anti-Ki-67 (ThermoFisher, RM-9106-S1, 1:100–1:500); anti BrdU (AbD Serotec, MCA2060, clone 1G9,3G5 (mixed), 1:250–1:500); anti-amylase (Sigma, A8273, 1:250–1:1,000); anti-SOX9 (Millipore, AB5535, clone 2B10, 1:100–1:500); phospho-p44/42 MAPK (ERK1/2) (Cell Signaling, 4370, clone D13.14.4E, 1:250–1:1,000); phospho-p44/42 MAPK (ERK1/2) (Cell Signaling, 4376, clone 20G11, 1:250–1:1,000); anti-insulin (Sigma, 273A, 1:250–1:1,000); anti-MUC5A (ThermoFisher, MS-145-P0, clone 45M1, 1:500); anti-DCLK1 (Abcam, ab31704, 1:250) and anti-BMI1 (Bethyl, A301–694A, 1:250–1:500).

Secondary antibodies used were purchased from Jackson ImmunoResearch and used at 1:500 dilution. Peroxidase AffiniPure Goat Anti-Mouse IgG, light chain specific (115–035-174), Alexa Fluor 488 AffiniPure Donkey Anti-Guinea Pig IgG (H+L) (706–545-148), Peroxidase AffiniPure Donkey Anti-Rat IgG (H+L) (712–035-153), Alexa Fluor 488 AffiniPure Donkey Anti-Rat IgG (H+L) (712–545-153), Alexa Fluor 488 AffiniPure Donkey

Anti-Rat IgG (H+L) (712–545-153), Cy3 AffiniPure Donkey Anti-Rabbit IgG (H+L) (711–165-152) and Peroxidase AffiniPure Donkey Anti-Rabbit IgG (H+L) (711–035-152).

For analysis on cytospun samples, cells were sorted by FACS and cytospun (500 rpm for 5 min) onto slides. Slides were fixed in 4% (v/v) PFA for 20 min, and processed for single-molecule RNA FISH using an RNAscope 2.0 HD Detection-RED kit (ACDbio) according to the manufacturer's instructions. Cells with 0–2 foci of *Tert* mRNA were defined as Tert^{low} acinar cells and cells with more than 2 foci were defined as Tert^{high} acinar cells. Alcian blue staining for mucins was performed with nuclear Fast Red as the counter-stain after antibody staining, using a staining kit (IHC World), according to the manufacturer's instructions.

FACS

To obtain single cell suspension mice were euthanized, pancreata were collected and immediately placed in 7 ml digestion solution (per pancreas) containing 2 mg ml^{-1} Collagenase VIII (Sigma) and 0.2 mg ml^{-1} Trypsin inhibitor (Sigma). Pancreata were incubated for 10–12 min in a shaker at 37 °C. Cells were resuspended with FACS buffer (2% FBS in PBS) and filtered through a 100-μm cell strainer. Red blood cells were removed using red blood cell lysis buffer (Ebioscience) for 10 min at room temperature. Cells were incubated with anti-CD45 antibody (Biolegend, 103116, clone 30-F11, 0.25 μg per million cells) for 45 min. Cells were sorted with a BD Aria II flow cytometer using a 100-μm nozzle using BD FACSDiva software v8.0. Dead cells were excluded based on DAPI (1 μM) incorporation. FACS data were analysed using Flowjo (8.7).

Imaging analysis

Fluorescent images were analysed using Leica LAS AF, ImageJ (2.1.0) and Adobe Photoshop (CS6). Stitched images were processed from individual tiles by Adobe Photoshop. Ki67$^+$ and BrdU acinar cell nuclei were manually counted. Immunohistochemistry images were analysed with Leica LAS 4.2, ImageJ and Adobe Photoshop. Statistical significance was determined by one-tailed unpaired two-sample *t*-test. Plots were generated by the ggplot2 package (3.2.1) in R Studio (1.2.5019) and Graphpad Prism (8.7).

LCM and mutation screening

LCM of pancreatic sections was performed using an Arcturus PixCell IIe laser capture microdissection system. Phospho-ERK 1/2 positive and negative acinar cells from PDAC, chronic pancreatitis, SCA, MCN patients and autopsies were collected on CapSure Micro LCM caps (Applied Biosystems). For each of the pERK-positive regions, adjacent tissue sections were stained with haematoxylin and eosin and acinar morphology was confirmed by a pathologist. DNA was extracted using the PicoPure DNA extraction Kit according to the manufacturer's instructions (Applied Biosystems). Following incubation, proteinase K was inactivated by incubation at 95 °C for 10 min, and 1-μl aliquots of DNA were used for PCR analysis. PCR was performed for detection of wild-type and mutated *KRAS* G12/13 (Kras-G12_F: aggcctgctgaaaatgactg; Kras-G12_R: ttggatcatattcgtccacaa).

Libraries were prepped using Kapa Hyperprep Kit (Kapa KK8504), quantified with Qubit and bioanalyzer, and run on Illumina miSeq at the Stanford Functional Genomics Facility. Reads were checked for quality using FastQC and then paired using fastq-join tool at Galaxy (https://usegalaxy.org, version1.1.2-806.1). *KRAS* variants were identified using custom Python scripts (https://github.com/cmroake/KRAS_scripts) and the number of reads per variant was normalized to total *KRAS* reads. Kras mutations <5% were excluded to rule out potential contamination by non-acinar cells. This study protocol was approved by the Stanford University Institutional Review Board (Protocol #42887).

RT–qPCR

RT–qPCR was performed on TERT^{high} and TERT^{low} acinar cells isolated by FACS from five *Tert$^{CreERT2/+}$; Rosa26$^{LSL-Tomato/+}$* mice ten days after tamoxifen (5 mg) oral gavage. Acinar cells were sorted into lysis buffer (Macherey Nagel). Total RNA was extracted and purified using NucleoSpin XS (Macherey Nagel) according to the manufacturer's protocol. Quantitative PCR was performed using the following primers: *Tert* (TGGCTTGCTGCTGGACACTC/TGAGGCTCGTCTTAATTGAGGTCTG); *Amy2a* (TGCAGGTCTCTCCACCCAATGAAA/TGCACCTTGTCACCATG TCTCTGA); *Ptf1a* (TGCGCTTGGCCATAGGCTACATTA/AGATGATAACCTT CTGGGCCTGGT); *Actb* (TCGAGTCGCGTCCACC/GGGAGCAT CGTCGCCC). Quantitative PCR reactions (three technical replicates) were carried out using Brilliant II SYBR Green master mix (Agilent) and Roche lightcycler 480. Quantification cycle (C_q) values were determined by the second derivative maximum method, and fold-changes were calculated by $2^{-\Delta C_q}$.

Quantification of metaplastic and PanIN area

Haematoxylin and eosin slides of *Tert$^{CreERT2/+}$; Rosa26$^{LSLTomato/+}$; Kras$^{LSL-G12D/+}$* mice and *Ptf1a$^{CreERT2/+}$; Rosa26$^{LSLTomato/+}$; Kras$^{LSL-G12D/+}$* mice were scanned and metaplastic and PanIN areas were evaluated by a pathologist in a blinded manner. Metaplastic and PanIN area was calculated by dividing through total pancreatic area.

Quantification of clones per area

To quantify number of clones per 20× image Tomato-stained slides of *Tert$^{CreERT2/+}$; Rosa26$^{LSLTomato/+}$; Kras$^{LSL-G12D/+}$* mice and *Ptf1a$^{CreERT2/+}$; Rosa$^{26LSLTomato/+}$; Kras$^{LSL-G12D/+}$* mice were analysed for Tomato$^+$ clones per high-power field (HPF) (7 mice and 8 HPFs per mouse for each genotype).

Quantification of cells per clone

Tomato-stained slides of *Tert$^{CreERT2/+}$; Rosa26$^{LSLTomato/+}$* mice, *Ptf1a$^{CreERT2/+}$; Rosa$^{26LSLTomato/+}$* mice, *Tert$^{CreERT2/+}$; Rosa26$^{LSLTomato/+}$; Kras$^{LSL-G12D/+}$* mice and *Ptf1a$^{CreERT2/+}$; Rosa$^{26LSLTomato/+}$; Kras$^{LSL-G12D/+}$* mice were analysed and at least 50 Tomato$^+$ clones were quantified for cells per clone.

Statistics

Statistical testing was done using GraphPad Prism software with the appropriate test for each experiment. When comparing two groups, *P* values were determined using two-sided

unpaired Mann–Whitney test for two-group comparisons. Mice were randomly assigned to each experimental or control group. Fisher's exact test was used to analyse the correlation between pERK status and *KRAS* mutations in patient specimens. Data are presented as mean ± s.d. in the text. Graphs were generated using the ggplot2 package in R and Graphpad Prism.

Reporting summary

Further information on research design is available in the Nature Research Reporting Summary linked to this paper.

Data availability

Sequencing data for *KRAS* variants is available with the SRA accession: PRJNA598774. All other data are available from the authors upon reasonable request. Source data are provided with this paper.

Code availability

Custom Python scripts used in this manuscript are available at (https://github.com/cmroake/KRAS_scripts).
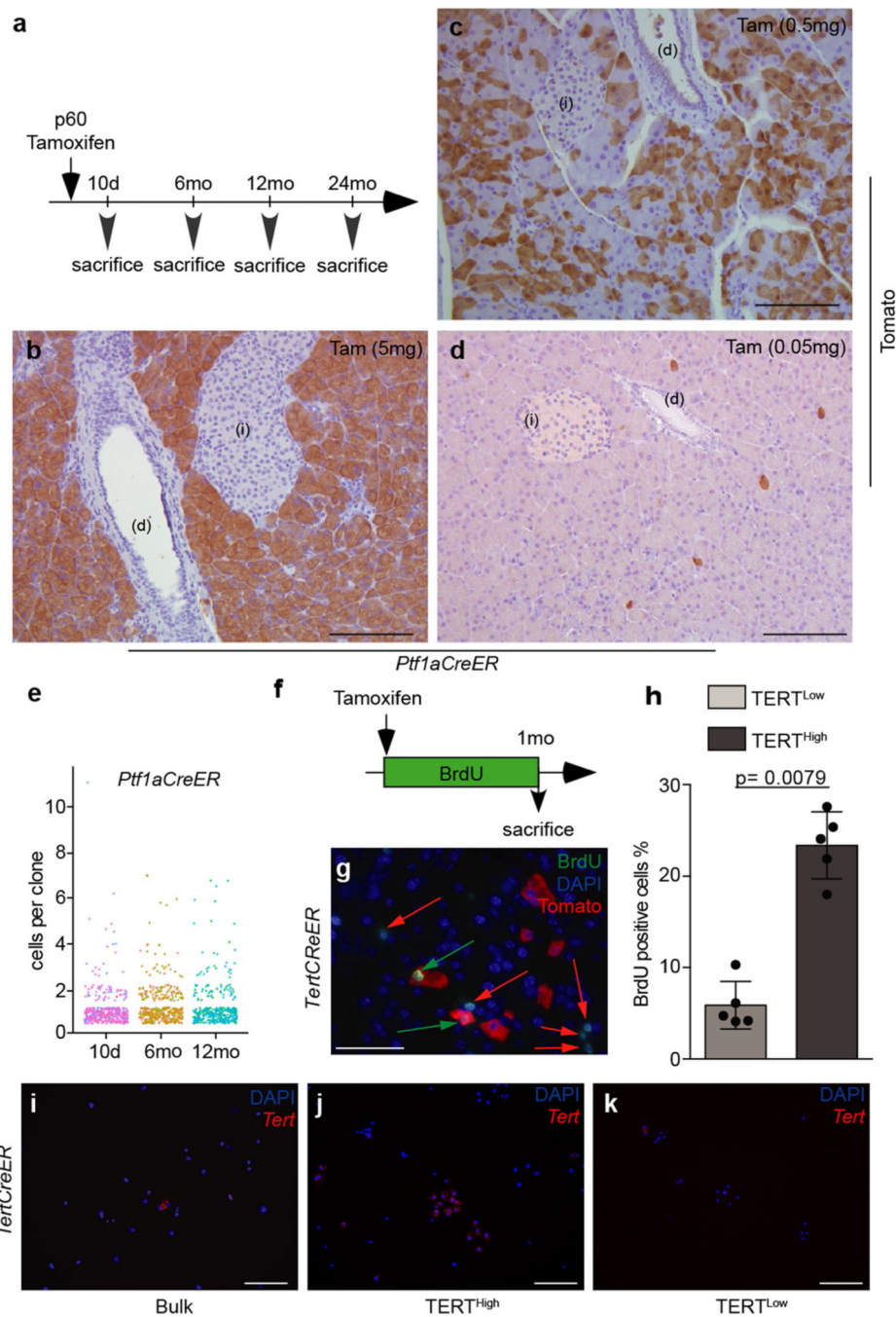
Extended Data
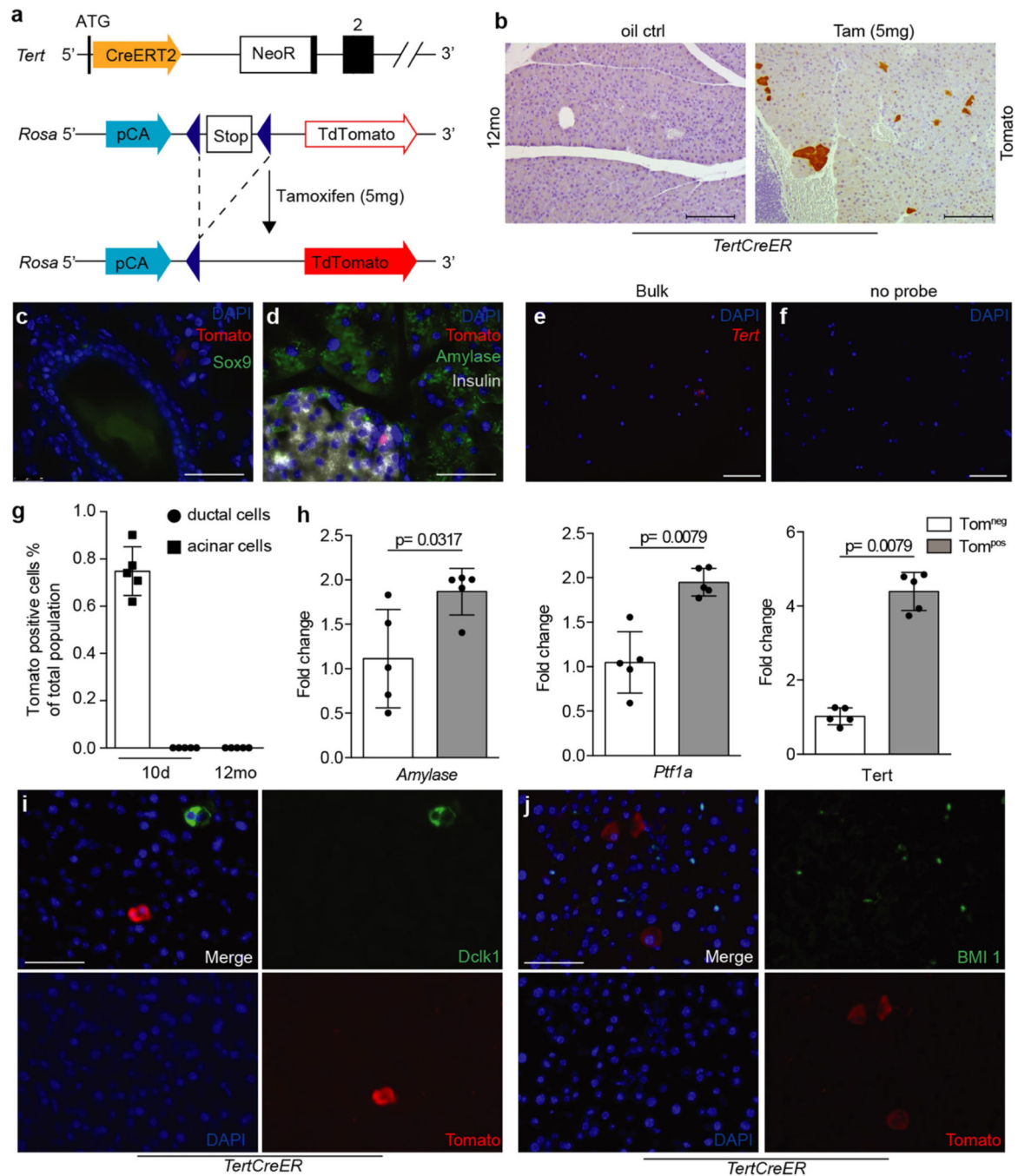
Extended Data Fig. 1 |. Identification of a TERT-high subpopulation in acinar cells and beta cells but not duct cells using lineage tracing.

a, $Tert^{CreERT2/+}; Rosa26^{LSL-tdTomato/+}$ mouse, which responds to tamoxifen-induced Cre-mediated activation of the tdTomato reporter allele. **b**, Immunohistochemistry analysis of Tomato in a $Tert^{CreERT2/+}; Rosa26^{LSL-tdTomato/+}$ (*TertCreER*) pancreas after oil and tamoxifen injection (n=4 mice for oil ctrl; n=11 mice for tamoxifen). Mo, month. **c, d**, Co-immunofluorescence stains 10 days after single dose of tamoxifen (5mg) in *TertCreER*

pancreas (n=4 mice). Tomato (red, **c**, **d**), DAPI (blue, **c**, **d**), Insulin (grey, **c**, **d**) Sox9 (green, **c**) and Amylase (green, **d**) are shown. **e**, **f**, Single-molecule RNA FISH for *Tert* mRNA (**e**) on FACS-purified bulk acinar cells (**e**, **f**) from *TertCreER* mice 10d after Tamoxifen (5mg) injection (n=4 mice). **g**, Quantification of Tomato-positive cells in *TertCreER* mice in the acinar cell compartment 10 days and within pancreatic ductal cells 10 days and 12 months post tamoxifen activation (n=5 mice). **h**, qRT-PCR for indicated genes in FACS-sorted Tom^{Neg} (white bars) and Tom^{Pos} (grey bars) acinar cells. **i**, **j**, Immunofluorescence analysis of a *TertCreER* pancreas 10 days after a single dose of 5mg tamoxifen (n=5 mice). Tomato (red), Dclk1 (**i**, green) or BMI1 (**j**, green) and DAPI (blue) are shown. Scale bar, 100μm (**b**), 50μm (**e**, **f**) and 25μm (**c**, **d**, **i**, **j**). All data are mean± SD. *P* values calculated by two-sided Mann-Whitney test (**h**).

Extended Data Fig. 2 |. Randomly marked acinar cells show limited clonogenicity and TERT-high acinar cells renew to yield TERT-low cells.

a, Schematic of lineage tracing in *TertCreER* mice treated with a single dose of tamoxifen on postnatal day 60 and analysis at indicated time points. Mo, month. **b–d**, Immunohistochemistry for Tomato in *Ptf1aCreER* mice 10d post tamoxifen (5mg (**b**), 0.5mg (**c**) and 0.05mg (**d**)) injection (n=4 mice). **e**, Distribution of Tomato-positive acinar cells per clone for each time point in *Ptf1aCreER* mice (each color represents one mouse; n=4 for each time point) **f**, *TertCreER* mice are injected with Tamoxifen (5mg) on postnatal

day 60 and put on BrdU water (1mg/ml) for 30 days. **g**, Immunofluorescence analysis of a *TertCreER* pancreas after 30 days of BrdU water. Tomato (red), BrdU (green) and DAPI (blue) are shown. TERT^{High} Tomato/BrdU double positive cells (green arrow) and TERT^{Low} BrdU positive cells (orange arrow) shown. **h**, Quantification of TERT^{Low} and TERT^{High} BrdU+ cells (n=5 mice) (mean ± SD). **i–k**, Single-molecule RNA FISH for *Tert* on FACS-purified bulk (**i**), TERT^{High} (**j**) and TERT^{Low} derived (**k**) acinar cells of *TertCreER* mice(n=3). Scale bars, 25μm (**g**), 50μm (**i–k**), 100 μm (**b–d**). *P* values calculated by two-sided Mann-Whitney test (**h**).
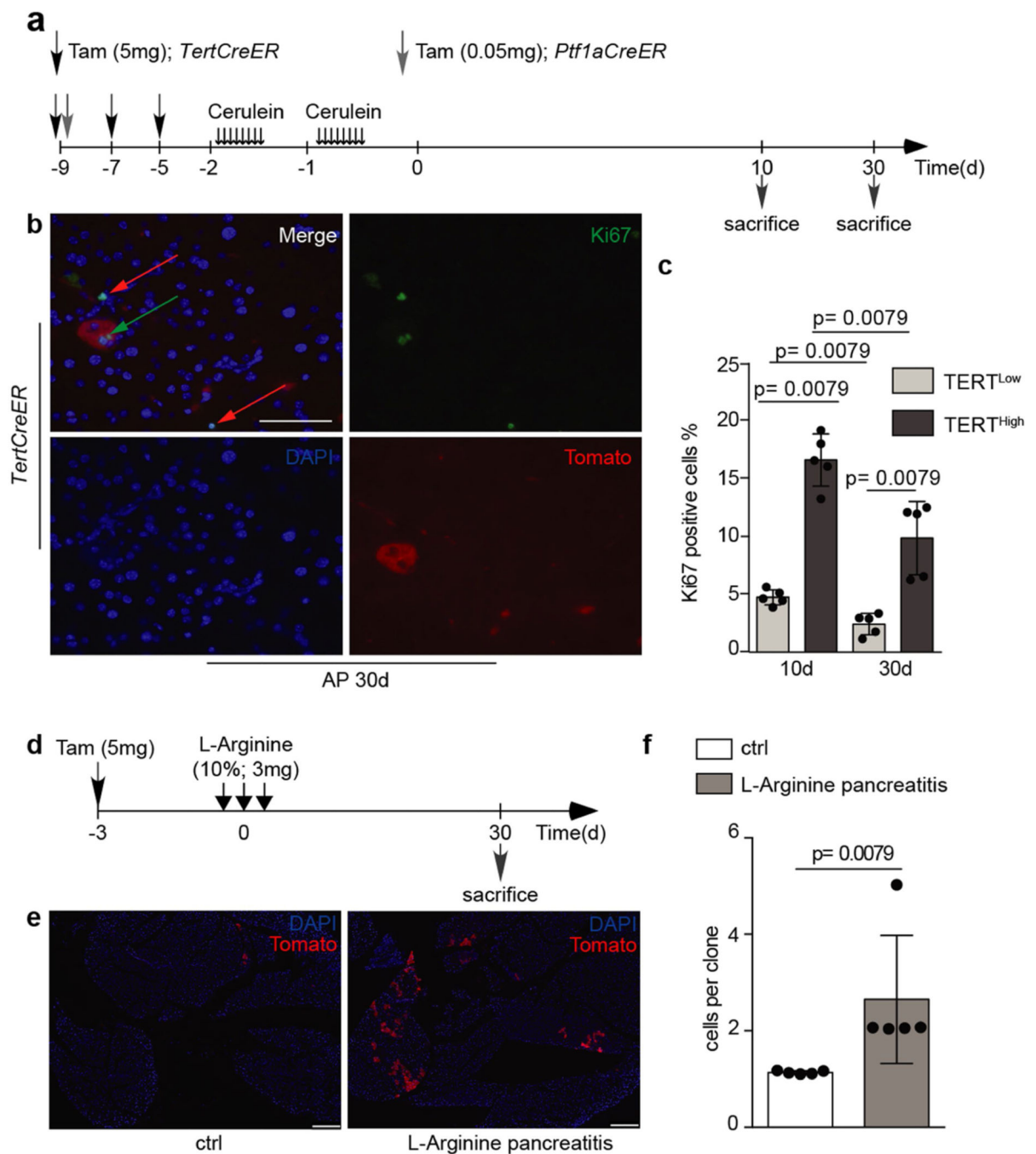
Extended Data Fig. 3 |. During injury, TERT^High acinar show enhanced repopulation compared with randomly marked acinar cells.

a, Schema of cerulein-induced pancreatitis. **b**, Immunofluorescence analysis of *TertCreER* mice 30 days after cerulein injections. Tomato (red), Ki67 (green) and DAPI (blue) are shown. TERT^High, Ki67+ positive cells (green arrow) and TERT^Low, Ki67+ cells (orange arrows) are shown. **c**, Quantification of TERT^High, Ki67+ and TERT^Low, Ki67+ cells at indicated time points (n=5 mice) (mean ± SD). **d**, Schematic of L-Arginine induced pancreatitis. **e**, Immunofluorescence analysis of *TertCreER* mice 30 days after L-Arginine

induced pancreatitis. **f**, Quantification of Tomato-positive cells per clone with and without injury (n=5 mice) (mean ± SD). Scale bars, 25μm (**d**), 250 μm (**e**). *P* values calculated by two-sided Mann-Whitney test (**c**, **f**).
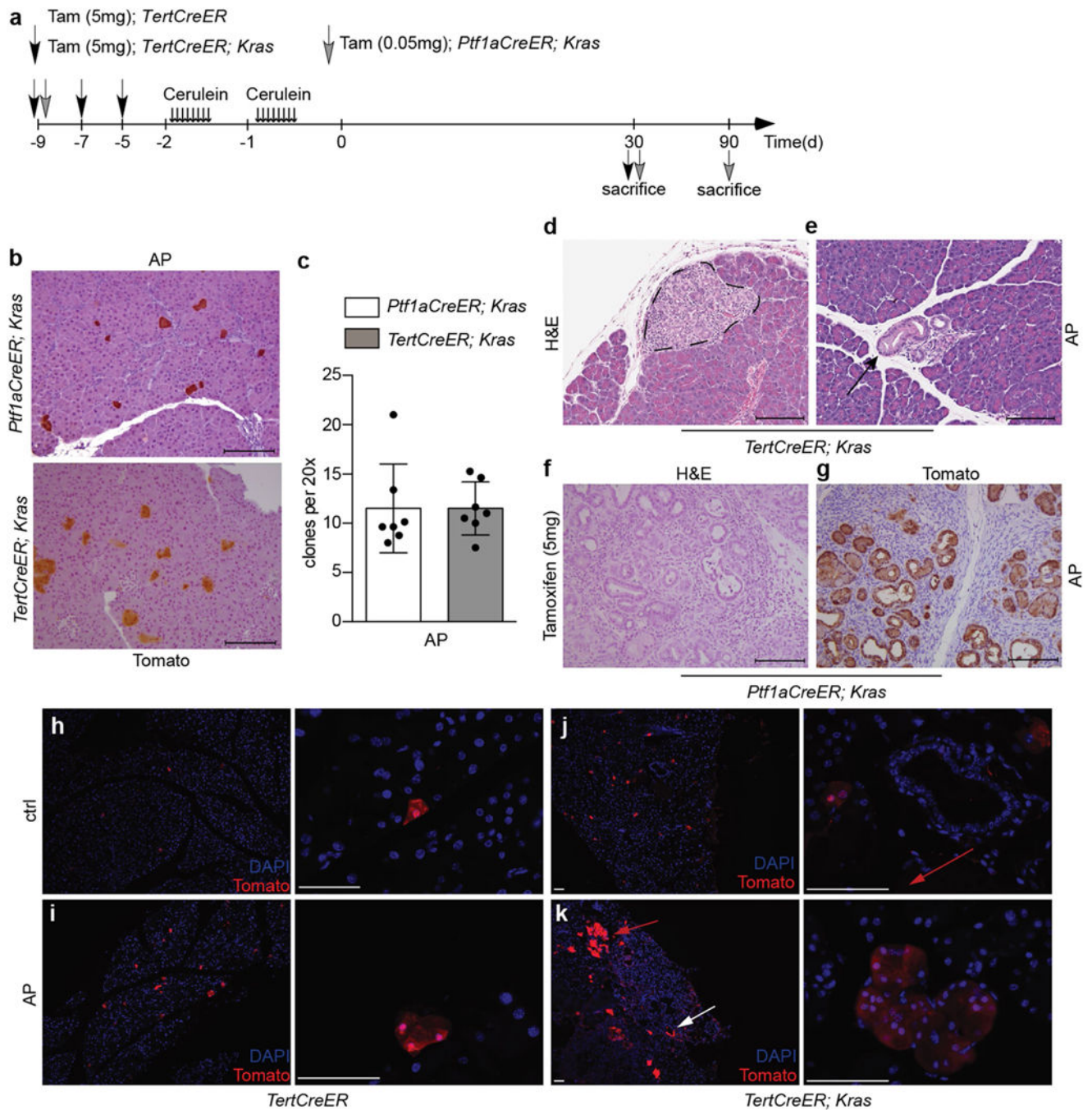
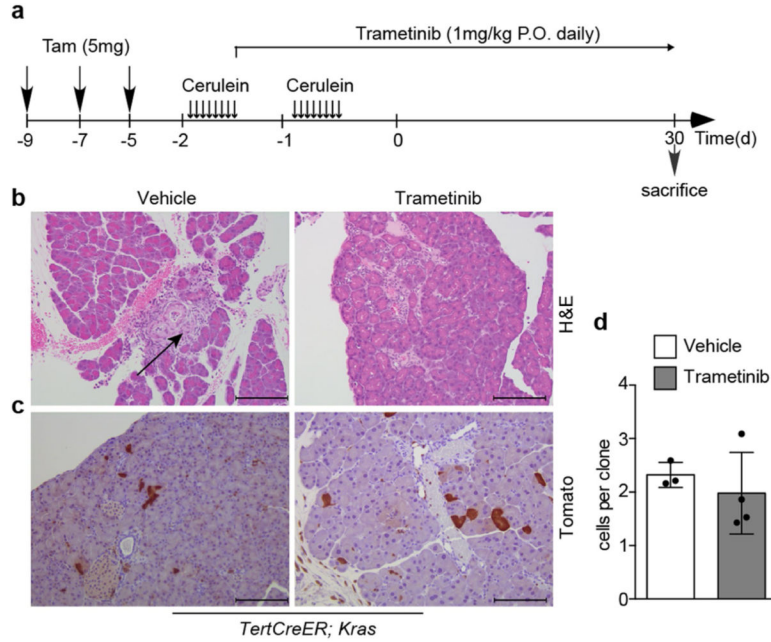**Extended Data Fig. 4 |. Enhanced PanIN formation from TERT-High acinar cells compared with sparsely labeled randomly marked acinar cells.**

a, Schema for cerulein-induced pancreatitis. **b**, Immunohistochemistry for Tomato in *Ptf1aCreER; Kras* mice and *TertCreER; Kras* mice one month after cerulein-induced pancreatitis (AP). **c**, Quantification of number of clones per 20x high-power field (HPF)

in *Ptf1aCreER; Kras* mice (n=7) and *TertCreER; Kras* mice (n=7) one month after cerulein-induced pancreatitis (AP) (mean ± SD). **d, e,** Representative metaplastic area (**d**, dashed line) and PanIN lesion (**e**, black arrow) in H&E staining of *TertCreER; Kras* mice one-month post injury (AP) (n=9 mice). **f, g,** Representative H&E staining (**f**) and Immunohistochemistry for Tomato (**g**) of Ptf1aCreER; Krasmice one-month post injury (AP) with high dose tamoxifen (5mg) (n=9 mice). **h–k,** Immunofluorescence analysis of a TertCreER (**h, i**) and TertCreER; Kras (**j, k**) mice one month after sham (**h, j**) or cerulein (**i, k**) treatment. Acinar cell expansion (red arrows) and PanINs (white arrow) are shown. Scale bar 100μm (**a, c–f**) and 50μm (**g–j**).

Extended Data Fig. 5 |. MEK inhibitor prevents PanIN formation from TERT-High cells expressing mutant Kras.

a, Schema of cerulein-induced pancreatitis with MEKi treatment (Trametinib). **b, c,** H&E (**b**) and Tomato (**c**) staining of *TertCreER; Kras* mice one month after cerulein induced pancreatitis with (Trametinib) and without (Vehicle) MEKi treatment. **d,** Quantification of Tomato-positive cells per clone with (n=4 mice) and without (n=3 mice) MEK inhibition (mean ± SD). Scale bars, 100μm.
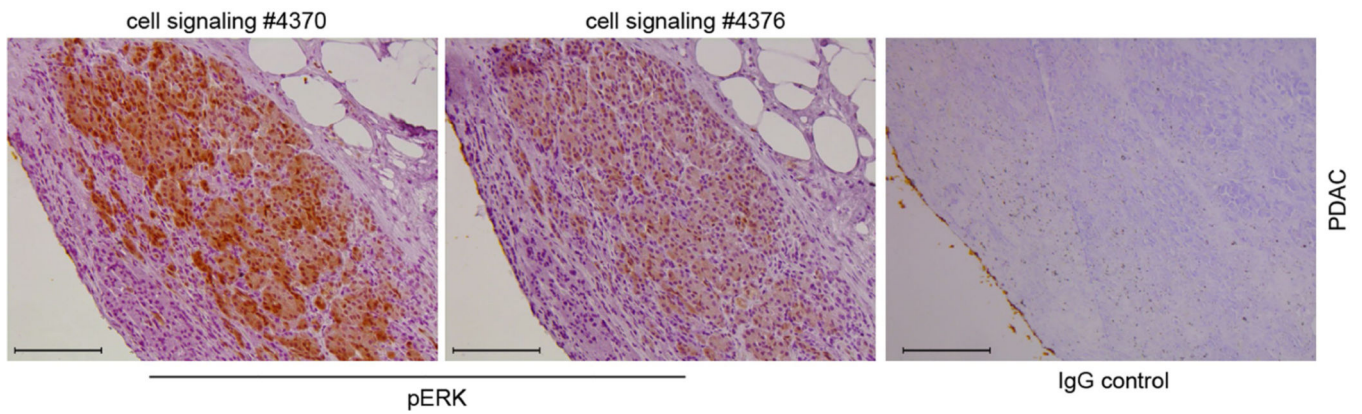
Extended Data Fig. 6 |. Specificity of pERK-positive acinar regions in human samples.
pERK 1/2 staining of human pancreas cancer specimen using indicated antibodies and IgG control (n=7 for #4376, n=44 for #4370 and n=3 for IgG control. Scale bars, 100μm.

Extended Data Table 1 |

Disease status of non-PDAC and autopsy samples

Patient	pERK status	WT %	Mutant %	Mutant Sequences (>1%)	Total Reads	Comments
Autopsy 1	negative	97	3	none	43414	
Autopsy 2	negative	97.6 ±0.7	2.4 ±0.7	none	212773	2 replicates
Autopsy 3	negative	97.8 ±0.5	2.2 ±0.5	none	219246	2 replicates
Autopsy 4	negative	97.5	2.5	none	37329	
Autopsy 6	negative	97.8 ±0.3	2.2 ±0.3	none	165620	2 replicates
Autopsy 7	negative	96.3	3.7	none	57472	
non-PDAC 1	negative	97.5	2.5	none	63348	
non-PDAC 2	negative	97.3	2.7	none	49771	
non-PDAC 3	negative	97.5	2.5	none	29657	
non-PDAC 5	negative	97.5	2.5	none	28758	
non-PDAC 6	negative	97.6	2.4	none	30768	
non-PDAC 7	negative	97.2	2.8	none	18889	
PDAC01	negative	97.6	2.4	none	36445	
PDAC 03	negative	97.4	2.6	none	5734	
PDAC 04	negative	97.2	2.8	none	39748	
PDAC 07	negative	94.6	5.4	G12S (2.9%)	53682	
PDAC 08	negative	97.5	2.5	none	53905	
PDAC 09	negative	98.3	1.7	none	91750	
PDAC 10	negative	97.5	2.5	none	50034	
PDAC 11	negative	97.2	2.8	none	68362	
PDAC 13	negative	97.8 ±0.11	2.2 ±0.12	none	256081	3 replicates
PDAC 14	negative	97.8	2.2	none	68957	
PDAC 15	negative	95.9	4.1	none	50064	
PDAC 17	negative	97.7 ± 0.35	2.3 ±0.35	none	185958	2 replicates

Patient	pERK status	WT %	Mutant %	Mutant Sequences (>1%)	Total Reads	Comments
PDAC 20	negative	37.3	62.7	L6F (60.3%)	33552	
PDAC 20 (area 2)	negative	98.3	1.7	none	66538	new area, same slide
PDAC 20 (area 3)	negative	95	5	G10V (2.9%)	83965	new area, same slide
PDAC 22	negative	97.5	2.5	none	28143	
PDAC 23	negative	96.4	3.6	none	94268	
PDAC 24	negative	7.5	92.5	G12D (80.8%), G12D/K16N (1.6%), G12D/G13C(1.1%)	116249	
PDAC 24 (area 2)	negative	98.1	1.9	none	83441	
PDAC 24 (area 3)	negative	98.3	1.7	none	115967	
PDAC 25	negative	91.7	8.3	G12D (3.5%)	130721	
PDAC 26	negative	98.2	1.8	none	128915	
PDAC 27	negative	97.9	2.1	none	135556	
PDAC 28	negative	94.1	5.9	G12D (4.1%)	158138	
PDAC 29	negative	96.5	3.5	V7L (1.7%)	148207	
PDAC 30	negative	95.2	4.8	L6I (2.0%), G12D(1.1%)	377806	
non-PDAC 1	positive	74	26	G12D (21.7%)	114886	
non-PDAC 2	positive	97.9	2.1	none	67988	
non-PDAC 3	positive	96.9	3.1	none	26565	
non-PDAC 4	positive	97.3	2.7	none	58276	
non-PDAC 6	positive	24.9	75.1	G12D (73.1%)	45951	
non-PDAC 9	positive	97.3	2.7	none	54690	
PDAC 01	positive	66.3	33.7	G12D (31.8%)	46942	
PDAC 02	positive	97.5	2.5	none	29584	
PDAC 07	positive	23.1	76.9	G12D (72.9%)	52310	
PDAC 10	positive	98.2	1.8	none	555230	
PDAC 11	positive	97.3	2.7	none	35462	
PDAC 14	positive	97.7	2.3	none	46224	
PDAC 15	positive	77.9	22.1	G12D (19.9%)	44781	
PDAC 17	positive	97	3	none	52614	
PDAC 18	positive	97.7	2.3	none	31605	
PDAC 22	positive	97.7	2.3	none	72487	
PDAC 29	positive	98	2	none	129653	
PDAC 31	positive	95.4	4.6	G12D (2.6%)	138413	

Mucinous cystic neoplasms (MCNs), Pancreatic Intraepithelial Neoplasia (PanIN), Hepatocellular carcinoma (HCC), Myelodysplastic syndromes (MDS), Bone Marrow Transplantation (BMT).

Extended Data Table 2 |

pERK status and Kras mutation sequences

Sample	Diagnosis
non-PDAC 1	serous cystadenoma
non-PDAC 2	MCN, pancreatitis (A1)
non-PDAC 3	Chronic pancreatitis with pseudocyst (A2-grossly uninvolved)
non-PDAC 4	serous cystadenoma, mild pancreatitis, PanlN-1a
non-PDAC 5	Chronic pancreatitis (adjacent to lymphoepithelial cyst)
non-PDAC 6	serous cystadenoma, pancreatitis, PanlN-2–3
non-PDAC 7	serous cystadenoma
non-PDAC 8	serous cystadenoma, focal PanlN-1a
non-PDAC 9	MCN (unremarkable pancreas adjacent)
Autopsy 1	metastatic breast ca complicated by aspiration pneumonia
Autopsy 2	MDS status post BMT complicated by multiple infections, secondary hemochromatosis
Autopsy 3	catatonic depression complicated by limb ischemia, pulmonary thromboemboli, aspiration pneumonia
Autopsy 4	coronary artery disease, CREST syndrome complicated by esophageal bleeding, colorectal cancer in remission
Autopsy 6	widely metastatic HCC complicated by pulmonary thromboemboli, tumor abutting but not invading pancreas
Autopsy 7	celiac disease complicated by enteropathy associated T cell lymphoma, severe Gl bleeding, status post initial chemo with fungal pneumonia

KRAS mutation sequence (>1%) of indicated patient samples with pERK status.

Supplementary Material

Refer to Web version on PubMed Central for supplementary material.

Acknowledgements

References

1. Rawla P, Sunkara T. & Gaduputi V. Epidemiology of pancreatic cancer: global trends, etiology and risk factors. World J. Oncol 10, 10–27 (2019). [PubMed: 30834048]

2. Jan M. et al. Clonal evolution of preleukemic hematopoietic stem cells precedes human acute myeloid leukemia. Sci. Transl. Med 4, 149ra118 (2012).

3. Barker N. et al. Crypt stem cells as the cells-of-origin of intestinal cancer. Nature 457, 608–611 (2009). [PubMed: 19092804]

4. Murtaugh LC & Keefe MD Regeneration and repair of the exocrine pancreas. Annu. Rev. Physiol 77, 229–249 (2015). [PubMed: 25386992]

5. Desai BM et al. Preexisting pancreatic acinar cells contribute to acinar cell, but not islet β cell, regeneration. J. Clin. Invest 117, 971–977 (2007). [PubMed: 17404620]

6. Westphalen CB et al. Dclk1 defines quiescent pancreatic progenitors that promote injury-induced regeneration and tumorigenesis. Cell Stem Cell 18, 441–455 (2016). [PubMed: 27058937]

7. Sangiorgi E. & Capecchi MR Bmi1 lineage tracing identifies a self-renewing pancreatic acinar cell subpopulation capable of maintaining pancreatic organ homeostasis. Proc. Natl Acad. Sci. USA 106, 7101–7106 (2009). [PubMed: 19372370]

8. Hruban RH, Goggins M, Parsons J. & Kern SE Progression model for pancreatic cancer. Clin. Cancer Res 6, 2969–2972 (2000). [PubMed: 10955772]

9. Kopp JL et al. Identification of Sox9-dependent acinar-to-ductal reprogramming as the principal mechanism for initiation of pancreatic ductal adenocarcinoma. Cancer Cell 22, 737–750 (2012). [PubMed: 23201164]

10. Habbe N. et al. Spontaneous induction of murine pancreatic intraepithelial neoplasia (mPanIN) by acinar cell targeting of oncogenic Kras in adult mice. Proc. Natl Acad. Sci. USA 105, 18913–18918 (2008). [PubMed: 19028870]

11. De La OJ et al. Notch and Kras reprogram pancreatic acinar cells to ductal intraepithelial neoplasia. Proc. Natl Acad. Sci. USA 105, 18907–18912 (2008). [PubMed: 19028876]

12. Flowers BM et al. Cell of origin influences pancreatic cancer subtype. Cancer Discov. 11, 660–677 (2021). [PubMed: 34009137]

13. Boj SF et al. Organoid models of human and mouse ductal pancreatic cancer. Cell 160, 324–338 (2015). [PubMed: 25557080]

14. Lee J. et al. Reconstituting development of pancreatic intraepithelial neoplasia from primary human pancreas duct cells. Nat. Commun 8, 14686 (2017). [PubMed: 28272465]

15. Kanda M. et al. Presence of somatic mutations in most early-stage pancreatic intraepithelial neoplasia. Gastroenterology 142, 730–733.e739 (2012). [PubMed: 22226782]

16. Shi C. et al. KRAS2 mutations in human pancreatic acinar-ductal metaplastic lesions are limited to those with PanIN: implications for the human pancreatic cancer cell of origin. Mol. Cancer Res 7, 230–236 (2009). [PubMed: 19208745]

17. Jones S. et al. Core signaling pathways in human pancreatic cancers revealed by global genomic analyses. Science 321, 1801–1806 (2008). [PubMed: 18772397]

18. Hingorani SR. et al. . Preinvasive and invasive ductal pancreatic cancer and its early detection in the mouse. Cancer Cell 4, 437–450 (2003). [PubMed: 14706336]

19. Ying H. et al. Genetics and biology of pancreatic ductal adenocarcinoma. Genes Dev. 30, 355–385 (2016). [PubMed: 26883357]

20. Roake CM & Artandi SE Regulation of human telomerase in homeostasis and disease. Nat. Rev. Mol. Cell Biol 21, 384–397 (2020). [PubMed: 32242127]

21. Pech MF et al. High telomerase is a hallmark of undifferentiated spermatogonia and is required for maintenance of male germline stem cells. Genes Dev. 29, 2420–2434 (2015). [PubMed: 26584619]

22. Petersen GM et al. A genome-wide association study identifies pancreatic cancer susceptibility loci on chromosomes 13q22.1, 1q32.1 and 5p15.33. Nat. Genet 42, 224–228 (2010). [PubMed: 20101243]

23. Lin S. et al. Distributed hepatocytes expressing telomerase repopulate the liver in homeostasis and injury. Nature 556, 244–248 (2018). [PubMed: 29618815]

24. Morris JPT, Cano DA, Sekine S, Wang SC & Hebrok M. Beta-catenin blocks Kras-dependent reprogramming of acini into pancreatic cancer precursor lesions in mice. J. Clin. Invest 120, 508–520 (2010). [PubMed: 20071774]

25. Pylayeva-Gupta Y, Grabocka E. & Bar-Sagi D. RAS oncogenes: weaving a tumorigenic web. Nat. Rev. Cancer 11, 761–774 (2011). [PubMed: 21993244]

26. Collins MA, Yan W, Sebolt-Leopold JS & Pasca di Magliano M. MAPK signaling is required for dedifferentiation of acinar cells and development of pancreatic intraepithelial neoplasia in mice. Gastroenterology 146, 822–834.e827 (2014). [PubMed: 24315826]

27. Bryant KL, Mancias JD, Kimmelman AC & Der CJ KRAS: feeding pancreatic cancer proliferation. Trends Biochem. Sci 39, 91–100 (2014). [PubMed: 24388967]

28. Martincorena I. et al. Somatic mutant clones colonize the human esophagus with age. Science 362, 911–917 (2018). [PubMed: 30337457]

29. Martincorena I. et al. Tumor evolution. High burden and pervasive positive selection of somatic mutations in normal human skin. Science 348, 880–886 (2015). [PubMed: 25999502]

30. Busque L. et al. Recurrent somatic TET2 mutations in normal elderly individuals with clonal hematopoiesis. Nat. Genet 44, 1179–1181 (2012). [PubMed: 23001125]

31. Madisen L. et al. A robust and high-throughput Cre reporting and characterization system for the whole mouse brain. Nat. Neurosci 13, 133–140 (2010). [PubMed: 20023653]

32. Jackson EL et al. Analysis of lung tumor initiation and progression using conditional expression of oncogenic K-ras. Genes Dev. 15, 3243–3248 (2001). [PubMed: 11751630]

33. Kopinke D. et al. Ongoing Notch signaling maintains phenotypic fidelity in the adult exocrine pancreas. Dev. Biol 362, 57–64 (2012). [PubMed: 22146645]

34. Hegyi P. et al. L-arginine-induced experimental pancreatitis. World J. Gastroenterol 10, 2003–2009 (2004). [PubMed: 15237423]
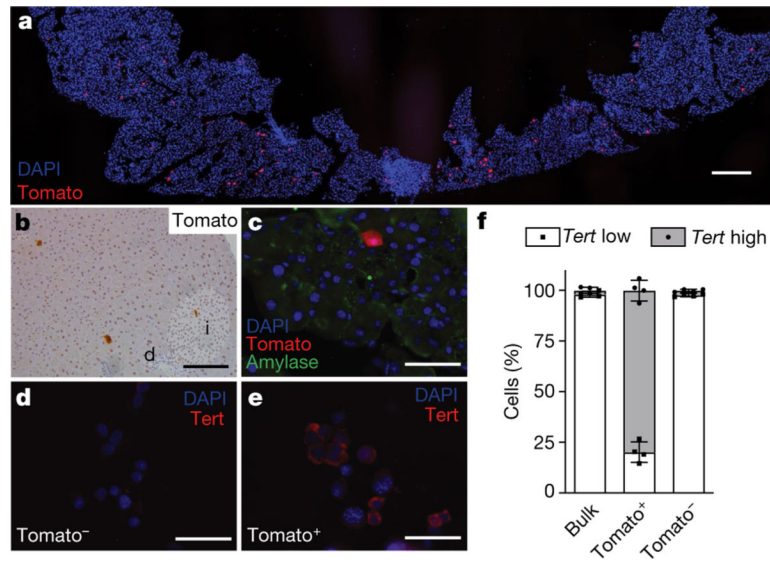
Fig. 1 |. Identification of an acinar cell subpopulation with elevated *Tert* expression.
a, **b**, Immunofluorescence (**a**; red, Tomato; blue, DAPI) and immunohistochemistry (**b**; i, islets; d, ducts; brown, Tomato; blue, haematoxylin) staining of pancreas of *Tert-CreER* mice 10 days after 5 mg tamoxifen treatment. **c**, Immunofluorescence staining 10 days after tamoxifen treatment (5 mg) in pancreas of *Tert-CreER* mice. Red, Tomato; blue, DAPI; green, amylase. **d**–**f**, Single-molecule RNA FISH for *Tert* mRNA (**d**) on FACS-purified Tomato$^-$ (**d**) and Tomato$^+$ acinar cells (**e**) from *Tert-CreER* mice 10 days after tamoxifen (5 mg) injection. **f**, Quantification of *Tert* expression in bulk wild-type acinar cells, Tomato$^+$ acinar cells and Tomato$^-$ acinar cells from **d**, **e**. Data are mean ± s.d. Scale bars, 250 μm (**a**), 100 μm (**b**), 50 μm (**c**), 25 μm (**d**, **e**). $n = 4$ mice (**a**–**f**).
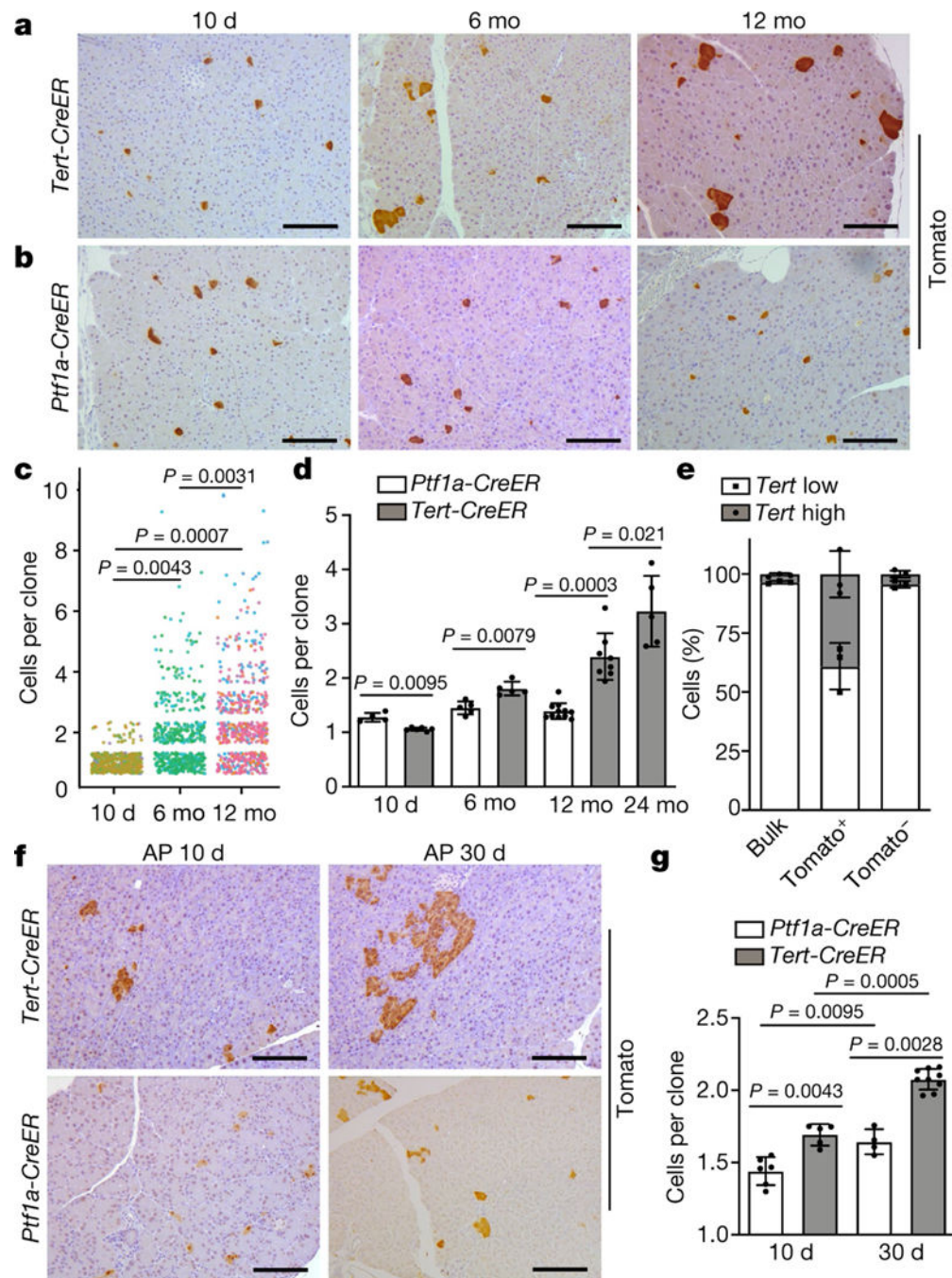
Fig. 2 |. TERT^high acinar cells repopulate the pancreas during homeostasis and regeneration.
a, **b**, Immunohistochemistry of Tomato⁺ cells in *Tert-CreER* mice (**a**) and *Ptf1a-CreER* mice
(**b**) at indicated time points after injection with 5 mg and 0.05 mg tamoxifen, respectively.
Mo, month. **c**, Distribution of Tomato⁺ acinar cells per clone in *Tert-CreER* mice (each
colour represents one mouse; $n = 6$ mice for 10 d; $n = 5$ mice for 6 mo and $n = 8$ mice for 12
mo). P values represent comparison of means of mice for each time point. **d**, Quantification
of Tomato⁺ cells per clone in *Ptf1a-CreER* mice (white bars) at 10 d ($n = 4$), 6 mo ($n = 5$)
and 12 mo ($n = 11$) and *Tert-CreER* mice (grey bars) ($n = 6$ for 10 d, $n = 5$ for 6 mo, $n =$

8 for 12 mo and $n = 5$ for 24 mo). Data are mean ± s.d. **e**, Quantification of RNA FISH for
Tert mRNA on FACS-purified bulk acinar cells, Tomato+ acinar cells and Tomato− acinar
cells 12 months after treatment of *Tert-CreER* mice with 5 mg tamoxifen ($n = 3$ mice). Data
are mean ± s.d. **f**, Immunohistochemistry analysis of *Ptf1a-CreER* and *Tert-CreER* mice
at indicated time points after cerulein-induced acute pancreatitis (AP). **g**, Quantification of
Tomato-positive cells per clone in *Ptf1a-CreER* mice (white bars) ($n = 6$ for 10 d, $n = 4$ for
30 d) and *Tert-CreER* mice (grey bars) ($n = 5$ for 10 d, $n = 9$ for 30 d) after injury. Data
are mean ± s.d. Scale bars, 25 μm (**a**), 100 μm (**b, c, f**). *P* values calculated by two-sided
Mann–Whitney test (**c, d, g**).
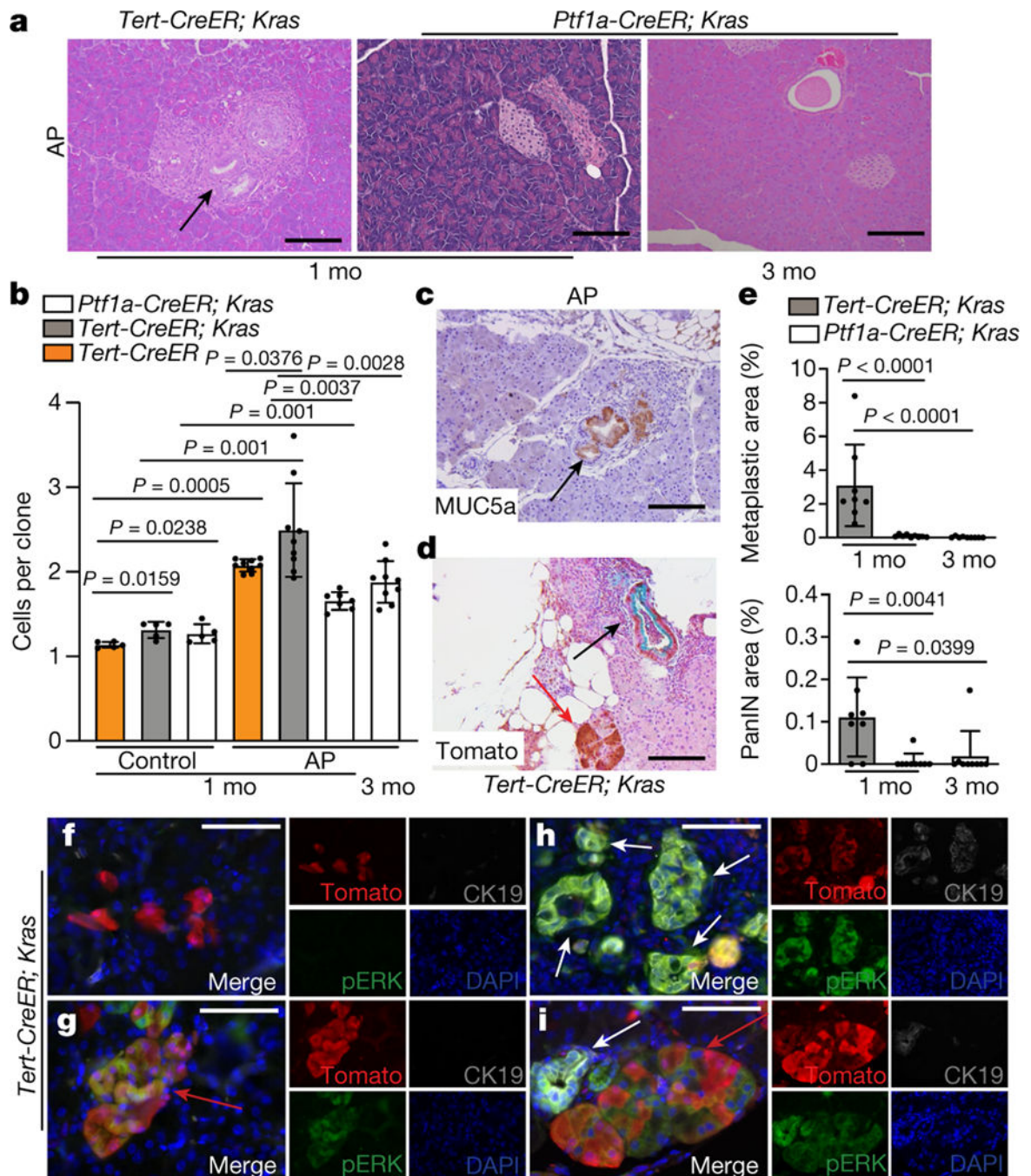
Fig. 3 |. TERT^high acinar cells initiate pancreatic neoplasia upon Kras activation and injury.
a, Haematoxylin and eosin staining of pancreas from *Ptf1a-CreER; Kras* mice and *Tert-CreER; Kras* mice after cerulein-induced acute pancreatitis. Black arrow indicates a PanIN lesion. **b**, Tomato-labelled acinar cell clone size in *Ptf1a-CreER; Kras* mice (white bars) ($n = 5$ for control, $n = 7$ for AP at 1 month and $n = 9$ for AP at 3 months), *Tert-CreER; Kras* mice (grey bars) ($n = 5$ for control, $n = 9$ for AP) and *Tert-CreER* mice (orange bars) ($n = 5$ for control, $n = 9$ for AP) after sham (control) and acute pancreatitis treatment. Data are mean ± s.d. The *Tert-CreER* mice (orange bars) are the same mice used in

Fig. 2 for acute pancreatitis. **c, d**, Immunohistochemistry staining of MUC5A (brown) (**c**), and Tomato (brown) and Alcian blue (blue) (**d**) in *Tert-CreER; Kras* mice one month after cerulein injections. Counterstains are haematoxylin (**c**) and Fast Red (**d**). PanIN lesions (black arrows) and acinar cell clones (red arrow) are shown. **e**, Quantification of metaplastic area and PanIN area in *Ptf1a-CreER; Kras* mice (white bars) ($n = 9$ for 1 and 3 months) and *Tert-CreER; Kras* mice (grey bars) ($n = 8$) relative to total pancreas area after cerulein (acute pancreatitis) treatment at indicated time points. Data are mean ± s.d. **f–i**, Immunofluorescence of *Tert-CreER; Kras* mice one month after induction of acute pancreatitis. Tomato (red), phospho-ERK 1/2 (green), cytokeratin 19 (grey) and DAPI (blue) are shown. Red arrows indicate acinar cell expansion and white arrows indicate PanINs are shown ($n = 4$ mice). Scale bars, 100 μm (**a, c, d**), 25 μm (**f–i**). *P* values calculated by two-sided Mann–Whitney test (**b, e**).
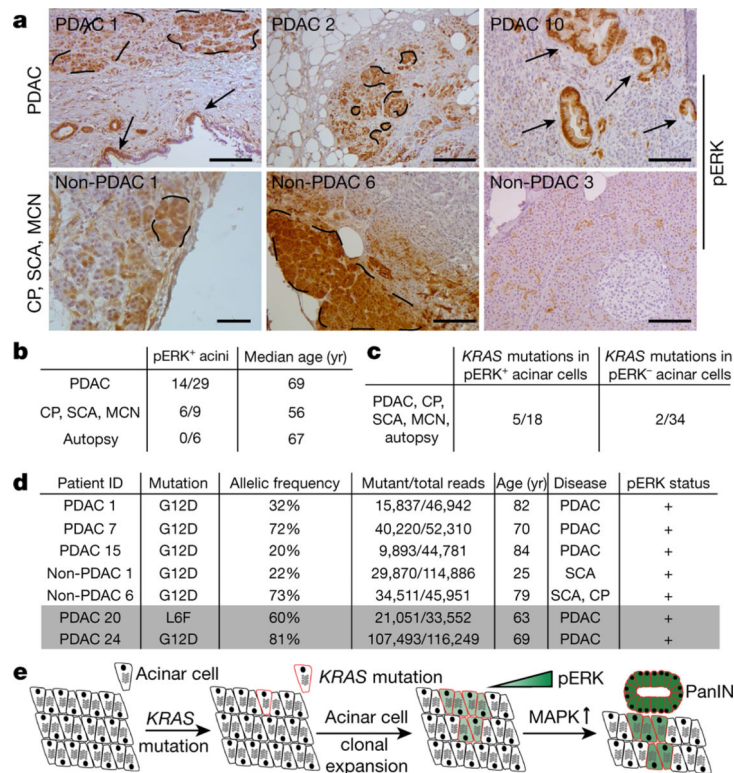
Fig. 4 |. Identification of pERK⁺ human acinar cells harbouring *KRAS* mutations.
a, Immunohistochemistry for pERK in resected samples of human PDAC, chronic pancreatitis (CP), serous cystadenoma (SCA) and mucinous cystic neoplasm (MCN). pERK⁺ acinar cells (dashed lines) and PanINs (black arrows) are shown. **b**, Quantification of pERK⁺ acinar cell areas in indicated patient groups (number of patients with pERK⁺ acinar areas/number of total patients). **c**, Sequencing results for *KRAS* mutations in DNA from pERK⁻ and pERK⁺ acinar cell areas isolated by LCM. **d**, Sequencing results from patients harbouring *KRAS* mutations. Shading indicates samples were from pERK⁻ regions. $P = 0.0409$, two-sided Fisher's exact test for *KRAS* mutations in pERK⁺ regions compared with *KRAS* mutations in pERK⁻ regions **e**, Proposed model of acinar cell clonal expansion and PanIN formation. Acinar progenitor cells sustain a *KRAS* mutation during replication, conferring a growth advantage and supporting formation of an acinar clone. *KRAS*-driven clones expand, yielding a field of abnormal cells, and transdifferentiate to a PanIN lesion. Ras–MAPK signalling is amplified during expansion and differentiation to the ductal fate. Scale bars, 100 μm.